YTUP

Journal of Thermal Engineering

https://jten.yildiz.edu.tr/

https://doi.org/10.47481/jten.0029

RESEARCH ARTICLE

Thermal performance of a lid-driven cavity with a rotating cylinder using encapsulated phase change materials and silica nanofluids

Farida Iachachene[1,2,*], Hanane Cheradi[2], Leila Saoudi [1,3], Ahmet Selim Dalkilic[4,5]

[1]Earth Physics Laboratory, Faculty of Hydrocarbon and Chemistry, University M'Hamed Bougara Boumerdes, Boumerdes 35000, Algeria
[2]LEMI (Laboratory of Energy, Mechanics and Engineering), Department of Mechanical Engineering, Faculty of Technology, University M'Hamed Bougara Boumerdes, 35000, Algeria
[3]Laboratory of Hydrocarbons Physical Engineering, Faculty of Hydrocarbons and Chemistry, University of M'Hamed Bougara Boumerdes, 35000, Algeria
[4]Department of Mechanical Engineering, Mechanical Engineering Faculty, Yildiz Technical University, Istanbul, 34349, Türkiye
[5]Scientific Research Department, Azerbaijan University of Architecture and Construction (AzUAC), Baku, AZ1073, Azerbaijan

Abstract

In this study, we numerically investigate the thermal behavior of two types of nanofluids under mixed convection, both subjected to the same operating conditions. One nanofluid contains nanoencapsulated phase change material particles with gallium cores and silica shells (Ga@SiO_2), while the other uses conventional SiO_2 nanoparticles. This approach enables us to assess the impact of the latent heat associated with the PCM core and provides a clearer understanding of its influence on heat transfer performance. The physical model is a square cavity with a top moving wall and a rotating inner cylinder. The analysis is performed for Richardson numbers between 0.1 and 100, while the nanoparticle concentration varies from 0% to 4%. A finite volume technique is employed to solve the governing equations for momentum and energy. Validation against published results confirms the accuracy of our numerical approach. It has been found that the Ga@SiO_2/water nanofluids perform better than the SiO_2/water nanofluids. At Ri = 10 and a particle fraction of 4%, the Ga@SiO_2/water nanofluid achieves a maximum heat transfer enhancement of 20.31%, whereas the SiO_2/water nanofluid only reaches 1.68%. The observed enhancement can be explained by the combined contribution of the phase change occurring within the gallium core, which allows energy to be absorbed and released. The addition of Ga@SiO_2 particles enhances heat transfer, making this suspension suitable for thermal applications.

Keywords: Mixed convection, NEPCM nanofluid, Ga@SiO_2, core-Shell, heat transfer enhancement, latent heat storage

Cite this article as: Iachachene, F., Hanane, C., Saoudi, L., & Dalkilic, A. S. (2026). Thermal performance of a lid-driven cavity with a rotating cylinder using encapsulated phase change materials and silica nanofluids. Journal of Thermal Engineering, 12(4), 1267–1281. https://doi.org/10.47481/jten.0029

1. Introduction

Efficient heat transfer in mixed convection systems plays a key role in improving thermal management in treatments such as solar energy storage, photovoltaic cooling, and industrial heat recovery [1-6]. Many studies have shown that adding nanoparticles, especially metallic or oxide ones, to a base fluid can improve its thermal behavior [7–12]. More recently, attention has shifted toward a different type of particles known as core–shell structures. In this configuration, when the core consists of a phase change material (PCM) enclosed within a protective shell, the particles are generally referred to as nano-encapsulated phase change materials (NEPCM). In the study, the notation PCM@shell is used to represent a core–shell structure, where PCM is the core material and shell acts as the encapsulating layer. These materials have attracted increasing interest in thermal engineering. The shell surrounding the PCM prevents leakage during melting and solidification and improves the overall stability and durability of the particles [13,14]. Because of these advantages, encapsulated PCMs are now widely investigated for applications involving heat transfer and thermal storage.

*Corresponding Author
E-mail Adress: f.iachachene@univ-boumerdes.dz

Submitted: 3 March 2026; **Accepted:** 31 May 2026

This paper was recommended for publication in revised form by Editor-in-Chief Ahmet Selim Dalkılıç

When such particles are dispersed in a base fluid, they form what is commonly called NEPCM slurries or latent heat nanofluids [15]. In this case, the fluid benefits not only from the presence of nanoparticles, but also from the latent heat associated with the phase change of the core material. The nature of the shell, whether polymeric, metallic, or inorganic, plays a valuable role in the overall behavior of the suspension [16].

Several studies have also examined how the characteristics of these particles affect their properties. Parameters such as the shell thickness, the core-to-shell ratio, and the particle shape have a noticeable influence on thermal conductivity, density, and heat capacity [17–20]. In general, encapsulation tends to reduce the latent heat in comparison to the pure PCM, since part of the volume is occupied by the shell [13]. On the other hand, the density usually increases with shell thickness, while the thermal conductivity strongly depends on the shell material. For instance, metallic coatings often enhance heat transfer, whereas polymer-based shells may have the opposite effect [21]. These results highlight the need to improve the structural design of NEPCM nanoparticles to achieve optimal thermal performance for energy storage and temperature regulation applications. Adding nanoparticles PCM@shell to conventional liquids can effectively improve thermal performance. This improvement is due to the latent heat storage of coated PCM and the enhancement of the effective thermophysical properties of the suspension. In particular, the Nusselt number increases with optimized particle concentration and when T_m of the PCM@shell is near to the average wall temperature. These studies collectively display the ability of PCM@shell nanofluids to improve heat transfer under well-controlled conditions [22-27]. The present study focuses on Ga@SiO_2/water nanofluid under mixed convection conditions, a configuration that has received less attention compared to natural convection. Some recent works have nevertheless explored this type of structure and reported interesting thermal characteristics. For example, Ghalambaz et al. [28] studied the flow on a vertical surface and showed that reducing the melting temperature of the encapsulated material improves heat transfer. In another study, Ahmed and Raizah [29] evaluated the radiative and convective heat transfer in a prismatic cavity containing a NEPCM containing of a nonadecane core and a polyurethane shell. Their results indicate a significant increase in heat transfer in the presence of the NEPCM. Raizah et al. [30] used the ISPH technique to investigate mixed convection in a cylindrical hollow with lateral chambers and found that an increase in the radius of a revolving cylinder reduced the size of the melting area. Naseri Sadr et al. [31] studied mixed conviction of nanofluids with NEPCM. The physical model was a square cavity with a revolving heated cylinder. Latent heat effects and an increase in effective heat capacity improved heat transfer as the melting point approached a dimensionless value of 0.5, according to their results. Qasim et al. [32] also investigated convection coupled within a trapezoidal cavity influenced by wall ripples and an external magnetic field. They noted improved heat transfer with increasing Re and decreasing both the wall ripple quantity and the magnetic field strength. Herouz et al. [33] examined mixed convection of NEPCM inside a porous hexagonal enclosure and found that heat transfer was improved when the top and bottom walls moved in the identical way. However, lower permeability restricted fluid motion and diminished heat exchange between the thermal barriers. Iachachene et al. [34] investigated a computational investigation on mixed convection in a square cavity containing a rotating isothermal cylinder. They reviewed the impacts of magnetic field orientation and NEPCM nanofluid. The outcomes indicate that the adding of NEPCM enhanced heat transfer by more than 20%, with optimal melting points between 0.3 and 0.6, and that certain combinations of magnetic field angle and Ri produced localized increases of up to 3.34%. More recently, Dahani et al. [35] explored mixed convection heat transfer in a cavity filled with NEPCM nanofluids and a centrally placed rotating heated cylinder. They found that increasing the NEPCM volume percentage to 5% increased heat transmission by up to 14.92%, with the highest performance recorded at a fusion temperature of 0.45 for Ri = 100 and a cylinder radius of 0.2.

According to the available literature, in our knowledge no previous study has reported a direct comparison between NEPCM nanoparticles and conventional solid nanoparticles dispersed in a base fluid under similar mixed-convection conditions. The newness of the present investigation therefore lies in distinguishing the thermal contribution of latent-heat storage from that of solid nanoparticles alone. In this context, two suspensions are examined, Ga encapsulated within a SiO_2 shell (Ga@SiO_2) and SiO_2 nanoparticles dispersed in the base fluid. The comparison aims to evaluate the impact of PCM incorporation on the thermophysical properties of the suspension and the resulting heat-transfer performance. Gallium is selected as the core one and is frequently employed as a thermal energy storage medium owing to its substantial heat of fusion, which denotes the quantity of heat necessary to liquefy a certain mass of the substance. It has a significant heat of fusion, enabling it to absorb substantial heat for the period of melting and releases the accumulated heat upon solidification and it has commendable thermal conductivity. Furthermore, it is non-toxic, causing it to be suitable for diverse uses [36]. The silica (SiO_2) is used as shell material because of its chemical stability.

2. Mathematical formulation

2.1. Physical model

In this investigation, the physical model consists of a square cavity of height H, as illustrated in Figure 1. The upper horizontal wall moves with a constant velocity u_p and is kept at a uniform cold temperature T_c , while the lower horizontal wall is stationary and kept at a uniform hot temperature T_h. A circular cylinder is located at the center of the cavity, rotates with a constant angular velocity ω; its surface is kept at a constant temperature T_c.

Within this configuration, two different types of nanofluids are investigated. In the first configuration, the cavity is supplied with a conventional nanofluid having SiO_2 nanoparticles uniformly dis-

persed in the base fluid. In the second configuration, a novel class of nanofluids is examined, namely NEPCM-based nanofluids, in which the nanoparticles consist of a PCM(Ga) core encapsulated by a SiO_2 shell. The enclosure keeps PCM structure stable and lets latent heat be stored and released during the phase shift. These two types of nanofluids will be studying under the same geometric, thermal, and dynamic conditions to compare and evaluate how standard SiO_2 nanoparticles and PCM@SiO_2 core–shell nanoparticles affect the flow structure and heat transfer characteristics inside the cavity.

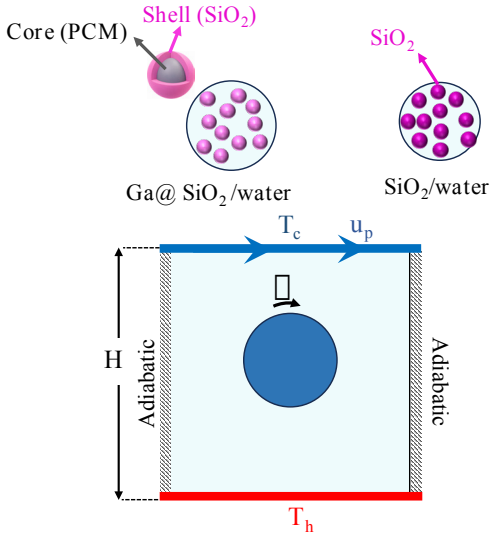

Figure 1. Physical model

2.2. Thermophysical properties of nanofluids

The thermophysical characteristics of the base fluid, core material (Ga), and shell material (SiO_2) are presented in Table 1. Gallium possesses a T_m= 302.93 K and L_f =801.6 kJ/kg.

Table 1. Thermophysical properties of base fluid, core, and shell materials [34]

Material Proprieties	water	Ga	SiO_2
Cp (J/kg·K)	4179	381.5	745
k (W/m·K)	0.613	32	1.4
ρ (kg/m3)	997.1	6093	2220
μ (kg/m·K)	$8.91^{-}10^{-4}$	–	–
β (1/k)	21□10^{-5}	22□10^{-5}	5.5 10^{-5}

2.3. Case of Nanofluid SiO_2/Water

The density of nanofluids containing SiO_2 nanoparticles is shown below:

$$\rho_{nf} = (1 - \varphi)\rho_f + \varphi\rho_{SiO_2} \quad (1)$$

The following is defined in terms of the principle of energy conservation, which accounts for the thermal equilibrium between the pure fluid and the particles:

$$C_{p,nf} = \frac{(1 - \varphi)(\rho C_p)_f + \varphi(\rho C_p)_{SiO_2}}{\rho_{nf}} \quad (2)$$

The effective thermal conductivity of nanofluids is specified as:

$$k_{nf} = \frac{2k_f + k_{SiO_2} + 2\varphi(k_{SiO_2} - k_f)}{2k_f + k_{SiO_2} - \varphi(k_{SiO_2} - k_f)} k_f \quad (3)$$

The dynamic viscosity of the nanofluids was evaluated using the Brinkman correlation:

$$\mu_{nf} = \mu_f (1 - \varphi)^{-2.5} \quad (4)$$

For the thermal expansion coefficient β_{nf} is given by:

$$\beta_{nf} = (1 - \varphi)\beta_f + \varphi\beta_{SiO_2} \quad (5)$$

2.4. Case of Nanofluid Ga@SiO_2/Water

The density of nanofluids with Ga@SiO_2 nanoparticle is stated below:

$$\rho_{nf} = (1 - \varphi)\rho_f + \varphi\rho_{Ga@SiO_2} \quad (6)$$

where, the density of nanoparticle with shell and core are given by [27,15]:

$$\rho_{Ga@SiO_2} = \frac{(1 + l_{SiO_2/Ga})\rho_{SiO_2}\rho_{Ga}}{\rho_{SiO_2} + l_{SiO_2/Ga}\rho_{Ga}} \quad (7)$$

where $l_{\{Si-\frac{O_2}{G}a\}}$ represents the shell-to-core weight ratio of the hybrid particle

Based on energy conservation theory and assuming the thermal equilibrium between the pure fluid and NEPCM, $C_{p,nf}$ is defined by:

$$C_{p,nf} = \frac{(1 - \varphi)(\rho C_p)_f + \varphi(\rho C_p)_{Ga@SiO_2}}{\rho_{nf}} \quad (8)$$

Total specific heat capacity $C_{p,Ga@SiO_2}$ of NEPCM, can be determined using the following equation [27,15]:

$$C_{p,Ga@SiO_2} = \frac{(C_{p,Ga} + l_{SiO_2/Ga}C_{p,SiO_2})\rho_{SiO_2}\rho_{Ga}}{(\rho_{SiO_2} + l_{SiO_2/Ga}\rho_{Ga})\rho_{p,Ga@SiO_2}} \quad (9)$$

Various heat capacity formulations, including rectangular (stepwise), triangular, and smooth functions, have been proposed in the literature to model the latent heat distribution in PCM systems [37]. In the present work, a sinusoidal profile is adopted due to its smooth behavior, which enhances numerical stability and avoids discontinuities.

The evaluation of the PCM heat capacity, as reported in [34, 38], accounts for its variation during the solid–liquid phase transition. Outside the phase change interval, an average value of the specific

heat capacity is considered based on the solid and liquid phases of gallium. Within the phase transition range, the latent heat effect is incorporated into the heat capacity formulation. In this study, the phase change procedure is modeled applying a sinusoidal function to represent the variation of $C_{p,Ga}$, following the procedure described in [34, 38]:

$$C_{p,Ga} = C_{p,Ga} + \left[\frac{\pi}{2}\left(\frac{L_{f,Ga}}{T_{liq} - T_{sol}} - C_{p,Ga}\right)\sin\pi\left(\frac{T - T_{sol}}{T_{liq} - T_{sol}}\right)\right]\delta \quad (10)$$

where the δ is

$$\delta = \begin{cases} 0 & T < T_{sol} \\ 1 & T_{sol} \leq T \leq T_{liq} \\ 0 & T > T_{liq} \end{cases} \quad (11)$$

This formulation ensures a smooth distribution of latent heat over the phase change temperature interval $[T_{sol}, T_{liq}]$, which helps to avoid numerical instabilities associated with abrupt property variations. It also allows the phase change process to be modeled without explicitly tracking the solid–liquid interface. Similar approaches have been widely adopted in PCM and NEPCM modeling studies [34, 38]. However, it should be noted that this method represents approximation, since the phase transition is distributed over a finite temperature range rather than occurring at a sharp interface.

The latent heat of the NEPCM is given by [15]:

$$L_{f,p} = \varphi_c \frac{\rho_c}{\rho_p} L_{f,c} \quad (12)$$

The effective thermal conductivity of nanofluids is stated as:

$$k_{nf} = \frac{2k_f + k_{Ga@SiO_2} + 2\varphi(k_{Ga@SiO_2} - k_f)}{2k_f + k_{Ga@SiO_2} - \varphi(k_{Ga@SiO_2} - k_f)} k_f \quad (13)$$

For isotropic core and shell materials, the mixing law for $k_{Ga@SiO_2}$ can be written as [15]:

$$k_{Ga@SiO_2} = \frac{(\rho_{SiO_2} k_{Ga} + l_{SiO_2/Ga}\rho_{Ga}k_{SiO_2})}{\rho_{SiO_2} + l_{SiO_2/Ga}\rho_{Ga}} \quad (14)$$

The dynamic viscosity of the nanofluids was evaluated using the Brinkman correlation:

$$\mu_{nf} = \mu_f (1 - \varphi)^{-2.5} \quad (15)$$

For the thermal expansion coefficient β_{nf} as given:

$$\beta_{nf} = (1 - \varphi)\beta_f + \varphi\beta_{Ga@SiO_2} \quad (16)$$

When both the shell and core materials are isotropic, the thermal expansion of core-shell nanoparticles can be decided using a mixing law. This law expresses the effective thermal expansion coefficient as a combination of the core and shell properties:

$$\beta_{Ga@SiO_2} = \frac{(\rho_{SiO_2}\beta_{Ga} + l_{SiO_2/Ga}\rho_{Ga}\beta_{SiO_2})}{\rho_{SiO_2} + l_{SiO_2/Ga}\rho_{Ga}} \quad (17)$$

2.5. Governing equations

To simulate mixed convection in nanofluid-filled cavities, a set of simplifying hypotheses is adopted. The dispersed nanoparticles ($Ga@SiO_2$ and SiO_2) are expected to be uniformly distributed within the base fluid and to remain in both thermal and kinematic equilibrium with it. Wholly thermophysical properties are considered temperature-independent, excluding density, which changes only in the buoyancy expression. For the NEPCM phase change material, the latent heat effect is unified using an effective heat capacity formulation over the melting temperature range. The remaining thermophysical properties are evaluated as effective temperature-independent values based on solid–liquid averages, as commonly adopted in NEPCM modeling studies [27-35]. The flow is accepted to be steady-state, incompressible, Newtonian, and two-dimensional. Furthermore, the influences of viscous dissipation and thermal radiation are ignored, as their contributions are expected to be negligible under the operating conditions considered. These assumptions allow the governing equations to be formulated in a tractable form while retaining the essential physical features of the problem. Therefore, the equations governing the mixed convection flow, under the adopted assumptions [34], are given as follows.

$$\frac{\partial u}{\partial x} + \frac{\partial v}{\partial y} = 0 \quad (18)$$

$$\rho_{nf}\left(u\frac{\partial u}{\partial x} + v\frac{\partial u}{\partial y}\right) = -\frac{\partial p}{\partial x} + \mu_{nf}\left(\frac{\partial^2 u}{\partial x^2} + \frac{\partial^2 u}{\partial y^2}\right) \quad (19)$$

$$\rho_{nf}\left(u\frac{\partial v}{\partial x} + v\frac{\partial v}{\partial y}\right) = -\frac{\partial p}{\partial y} + \mu_{nf}\left(\frac{\partial^2 v}{\partial x^2} + \frac{\partial^2 v}{\partial y^2}\right) + \rho_{nf} g\beta_{nf}(T - T_c) \quad (20)$$

$$(\rho C_p)_{nf}\left(u\frac{\partial T}{\partial x} + v\frac{\partial T}{\partial y}\right) = k_{nf}\left(u\frac{\partial^2 T}{\partial^2 x} + \frac{\partial^2 T}{\partial^2 y}\right) \quad (21)$$

where p denotes pressure, u and v refer to the x- and y- velocity, respectively. $k_{nf}, C_{p,nf}, \mu_{nf}, \rho_{nf}$, and β_{nf} represent the the thermal conductivity, the specific heat capacity, dynamic viscosity, density and the thermal expansion of nanofluid, correspondingly. The boundary conditions of this physical model are defined as follows:

Hot wall $(y = 0; 0 \leq x \leq H)$: $u = 0; v = 0; T = T_H$

Cold wall $(y = H; 0 \leq x \leq H)$: $u = 0; v = u_p; T = T_C$

Right adiabatic wall $(x = 0; 0 \leq y \leq H)$: $\left.\frac{\partial T}{\partial x}\right|_{x=0} = 0, u = v = 0$

Left adiabatic wall $(x = H; 0 \leq y \leq H)$: $\left.\frac{\partial T}{\partial x}\right|_{x=H} = 0, u = v = 0$

Rotating cylinder: $T = T_c, \omega_0 = 2u_p/d$

The equations (18)-(21) are converted by expressing them in a dimensionless form through the subsequent set of dimensionless parameters:

$$X = \frac{x}{H}, Y = \frac{y}{H}, U = \frac{u}{u_p}, V = \frac{v}{u_p}, P = \frac{pH^2}{\rho_f \nu_f u_p}, \theta = \frac{T - T_C}{T_H - T_C}$$

$$\rho^* = \frac{\rho_{nf}}{\rho_f}, c_p^* = \frac{C_{p,nf}}{C_{p,f}}, k^* = \frac{k_{nf}}{k_f}, \mu^* = \frac{\mu_{nf}}{\mu_f}, \beta^* = \frac{\beta_{nf}}{\beta_f}$$

The equations of continuity, momentum, and energy are represented in terms of the following non-dimensional parameters:

$$\frac{\partial U}{\partial X} + \frac{\partial V}{\partial Y} = 0 \quad (22)$$

$$\rho^* \frac{\partial}{\partial X}(UU) + \rho^* \frac{\partial}{\partial Y}(UV) = -\frac{1}{Re}\frac{\partial P}{\partial X} + \frac{\mu^*}{Re}\left[\frac{\partial}{\partial X}\left(\frac{\partial U}{\partial X}\right) + \frac{\partial}{\partial Y}\left(\frac{\partial U}{\partial Y}\right)\right] \quad (23)$$

$$\rho^* \frac{\partial}{\partial X}(UV) + \rho^* \frac{\partial}{\partial Y}(VV) = -\frac{1}{Re}\frac{\partial P}{\partial Y} + \frac{\mu^*}{Re}\left[\frac{\partial}{\partial X}\left(\frac{\partial V}{\partial X}\right) + \frac{\partial}{\partial Y}\left(\frac{\partial V}{\partial Y}\right)\right] + Ri(\rho^*\beta^*)\theta \quad (24)$$

The dimensionless parameters employed in this study are defined in Table 2.

$$\rho^* c_p^* \left(\frac{\partial}{\partial X}(U\theta) + \frac{\partial}{\partial Y}(V\theta)\right) = \frac{1}{PrRe}\left(\frac{\partial}{\partial X}\left(\frac{\partial \theta}{\partial X}\right) + \frac{\partial}{\partial Y}\left(\frac{\partial \theta}{\partial Y}\right)\right) \quad (25)$$

Table 2. Dimensionless parameters used in the study

Parameter	Symbol	Definition
Grashof, number	Ga	$Ga = \frac{g\beta_f (T_h - T_c) H^3}{\nu_f^2}$
Richardson number	Ri	$Ri = \frac{Gr}{Re_2}$
Prandtl numbers	Pr	$Pr = \frac{(C_p \mu)_f}{k_f}$
Reynolds number	Re	$Re = \frac{u_p H}{\nu}$

The local and average Nusselt numbers on the hot wall can be expressed as follows [34]:

$$Nu = -\frac{k_{nf}}{k_f}\frac{\partial \theta}{\partial Y}\Big|_{Y=0} \quad (26)$$

$$\overline{Nu} = \int_0^1 NudY \quad (27)$$

3. Numerical modelling

To solve the governing equalities (22) to (25) by their boundary conditions Numerical Methods and validation the finite volume technique is applied. The SIMPLE algorithm is employed to couple the velocity and pressure fields and to discretize the convection terms in the finite volume equalities, a second-order upwind scheme is adopted, while pressure discretization is handled through the PRESTO technique. An under-relaxation technique is employed to promote convergence, which is achieved when the absolute residual falls below 10^{-6}.

The convergence of the numerical solution is verified by monitoring the average Nusselt number along the hot wall as a function of the iteration number. As shown in Figure 2 for ϕ=2% and two Richardson numbers (Ri=0.1and Ri=100), $\overline{Nu}$ stabilizes beyond approximately 7000 iterations for Ri = 0.1 and 10000 iterations for Ri = 100, no significant change is observed, indicating that the solution has reached a converged state.

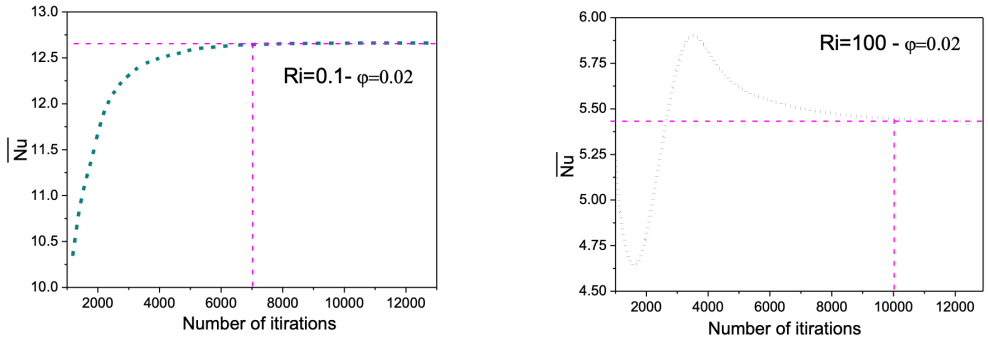

(a) **(b)**

Figure 2. Evolution of the average Nusselt number with iteration number for j=0.02 and different Ri

In addition, the convergence of the solution is verified by monitoring key physical quantities, such as , which remains unchanged with further iterations. The numerical uncertainty associated with spatial discretization is minimized through the grid independence study, where variations in the results are found to be negligible beyond a certain mesh resolution. These measures confirm the accuracy and stability of the numerical simulations.

The computational domain is discretized utilizing a structured, non-uniform mesh, as shown in Figure 3. The grid is refined in the vicinity of the cavity walls and around the cylindrical obstacle to better resolve the strong gradients of velocity and temperature that develop in these regions.

A grid independence test is then performed using six different meshes, with 6400, 14400, 25600, 40000, 48000, and 78400 cells. The influence of the mesh resolution is examined through the local Nusselt number along the heated wall (Figure 4), while the corresponding average values and relative deviations are summarized in Table 3. It is observed that the differences between successive refinements become very small, beyond 40000 cells. In particular, the variation in the average Nusselt number remains below 0.3%, indicating that the solution is no longer sensitive to further refinement. Based on these observations, the mesh with 40000 cells is retained as a suitable compromise between accuracy and computational effort.

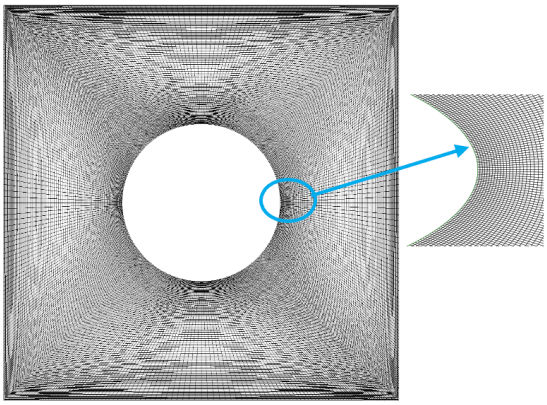

Figure 3. Mesh configuration

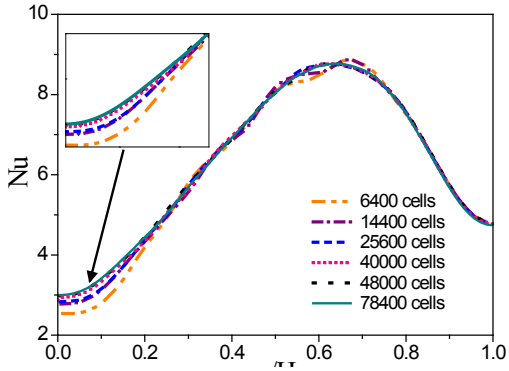

Figure 4. The grid Independence Test for Nu at Ri=10 for and j=0.02 and θ_f=0.6

Table 3. Effect of grid size on for Ri = 10 and j=0.02

Grid size	6400	14400	25600	40000	48000	78400
$\overline{Nu}$	6.5314	6.5922	6.6093	6.6298	6.6367	6.6454
Error	-	0.93%	0.26%	0.3%	0.01%	0.01%

The reliability and precision of the current numerical analysis are validated by comparing its results with those previously described by Khanafer and Aithal [39] for a rotating isothermal circular cylinder inside a square cavity. Figure 5a and 5b illustrate the comparison, showing the Nu distribution along the cavity's bottom surface and the horizontal velocity component along the vertical midplane, respectively. The high degree of concordance between the numerical results and the published data supports the validity and accuracy of the numerical code used in this research.

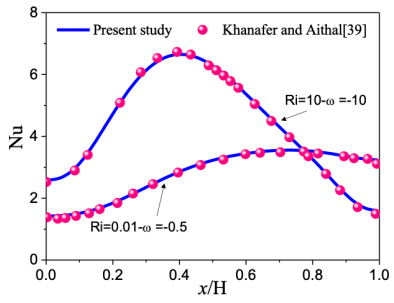

(a) Nusselt number variation along the hot wall

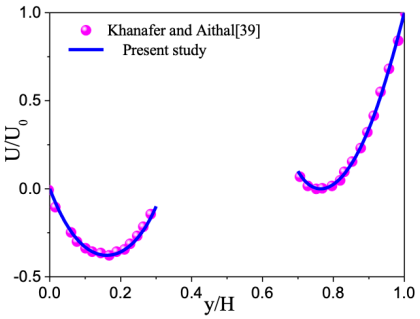

(b) Velocity in the horizontal direction at the vertical mid-plane for Re=100

Figure 5. Comparison of current results with those of Khanafer and Aithal [39]

In Figure 6(a-b), an additional validation is performed to assess the reliability of the computational technique through assessment with the practical data reported by Xu and Stock [40], who considered natural convection in a differentially heated cavity filled with gallium under the impact of a uniform magnetic field. In the present inquiry, only the case without a magnetic field considered corresponding to pure natural convection. The computed temperature and velocity profiles are in good harmony with the reference outcomes. The maximum relative deviation is approximately 0.2% for temperature and about 5% for velocity, indicating that the numerical approach provides satisfactory accuracy.

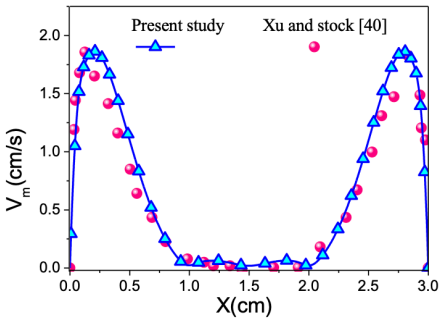

(a) Velocity magnitude along the line y=1.5cm

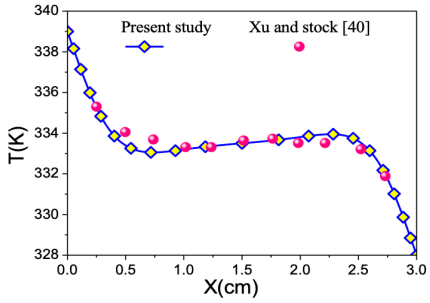

(b) Temperature distribution along the line y=1.5cm

Figure 6. Comparison of current outcomes with those of Xu and Stock [40]

Additionally, the NEPCM part of the model is justified through comparison with the work of Ghalambaz et al. [27]. Figure 7 demonstrates strong agreement in Nu at the hot wall under equivalent conditions, supporting the precision of the numerical method employed.

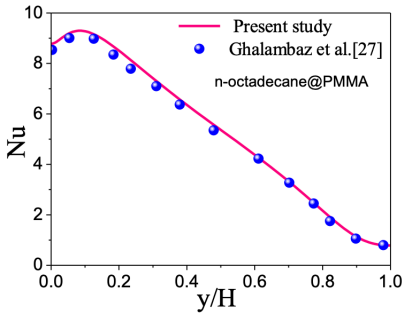

Figure 7. Comparison of Nu with findings stated in the literature [27] at Ra = 10^5 and $\theta_f = 0.3$

4. Results and discussion

4.1. Flow and thermal characteristics of Ga@SiO₂/Water Nanofluids

The numerical results for the Ga@SiO_2/Water nanofluid are presented in this section. The flow and thermal response of the nanofluid under dissimilar working conditions are studied. Simulations are performed for a range of Ri values and the effect of Ri and its influence on the flow structure and heat transfer behavior are examined.

The corresponding outcomes are demonstrated in Figure 8 which put forward the temperature contours and streamlines for Ri=0.1, 1, 10, and 100 at φ=2%. The results clearly indicate that Ri has a stated inpact on both the flow topology and the thermal field within the cavity. A dominant primary vortex is observed in all cases, whose position and intensity are governed by the relative contributions of forced convection induced by the moving lid and rotating cylinder, and buoyancy-driven natural convection. At low Ri (e.g., Ri=0.1), forced convection prevails, leading to a strong primary vortex accompanied by two secondary vortices forming near the lower corners of the cavity. These secondary vortices originate from buoyancy effects associated with temperature-induced density variations of Ga@SiO_2/Water. In the absence of lid motion and cylinder rotation, such buoyancy-driven vortices would occupy a larger portion of the cavity.

As Ri rises, the contribution of natural convection becomes more significant. As a result, the secondary vortex in the bottom left corner slowly weakens and is finally absorbed by the primary vortex. In this regime, buoyancy forces have more control over the movement of fluid in the lower part of the cavity. The upper zone flow is mainly driven by lid motion in combination with the rotation of the cylinder. The temperature distribution shows that the region is relatively cool and the higher temperature is localized near the bottom wall where forced convection dominates. The influence of buoyancy is more obvious at the bottom part of the cavity, but the flow field is still dominated by forced convection, especially on the right boundary. As the Ri increases, the high-temperature region on the left side expands further into the cavity. This trend is related to the decrease in mixing efficiency due to the increase of buoyancy forces. Meanwhile, the left region is subjected to improved heat removal owing to relatively higher local flow velocities which enable more effective convective heat transfer. Natural convection also acts a part in the temperature increase, but the coupling with the forced convection preserves an overall efficient heat transfer process. For Ri=100 corresponding to a regime of low Re, the ratio of maximum velocity (V_m/u_p) is about 1.4. Under such conditions the impact of the rotating cylinder on the flow dynamics is negligible while the buoyancy effects are dominating. So, the fluid motion and the consequent heat transfer are dominantly controlled by natural convection. The consequences denote that the flow structure and thermal performance are affected by the merged impacts of forced and natural convection, and the relative importance of the two is governed by parameters.

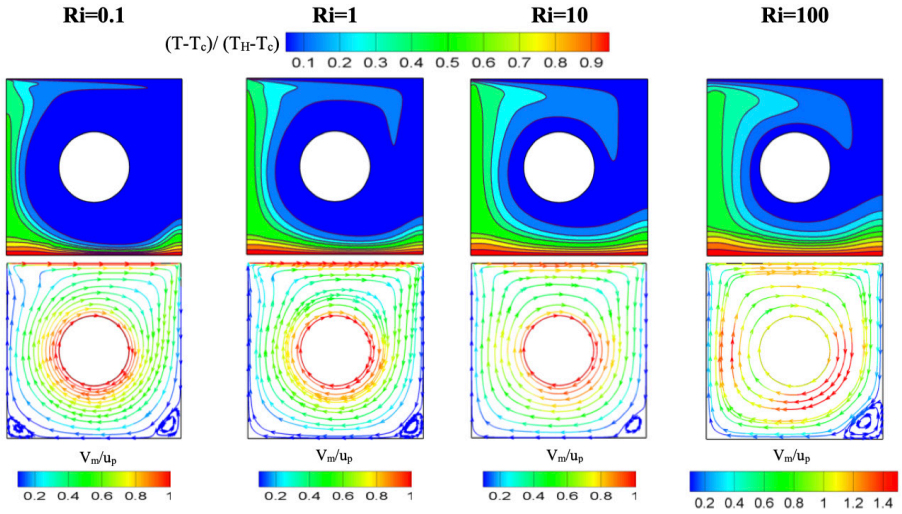

Figure 8. Effect of Ri on Temperature Distribution and Flow Patterns at Gr = 10^4 and ϕ = 2%

Figure 9. (a-c) illustrates the influence of the Ga@SiO_2/water volume fraction (0%, 2%, and 4%) on the flow structure and temperature distribution for dissimilar values of the Ri (0.1≤Ri≤100). At low Ri (Ri = 0.1), as illustrated in Figure 9a, the flow structure is only slightly affected by changes in the nanoparticle volume fraction j. In this situation, forced convection clearly plays a main role in driving the heat transfer process, with the highest velocities occurring near the moving lid and the rotating cylinder. Although adding Ga@SiO_2 nanoparticles doesn't significantly alter the overall flow pattern, it does enhance the thermal field, resulting in better heat transfer performance. As Ri increases, buoyancy effects gradually change both the velocity and temperature distributions inside the cavity. When Ri reaches 100, natural convection becomes dominant, leading to fluid velocities that surpass those generated solely by the moving

wall and rotating cylinder. Additionally, increasing j up to 4% leads to higher velocity magnitudes and a more uniform temperature distribution, which overall boosts heat transfer. The improved effective thermal conductivity and heat capacity are mainly due to the changes in the base fluid characteristics caused by the $Ga@SiO_2$ nanoparticles, which is the main reason for this enhancement. As a result, increasing the concentration of $Ga@SiO_2$ can substantially enhance the system's thermal performance, particularly in conditions where natural convection is dominant.

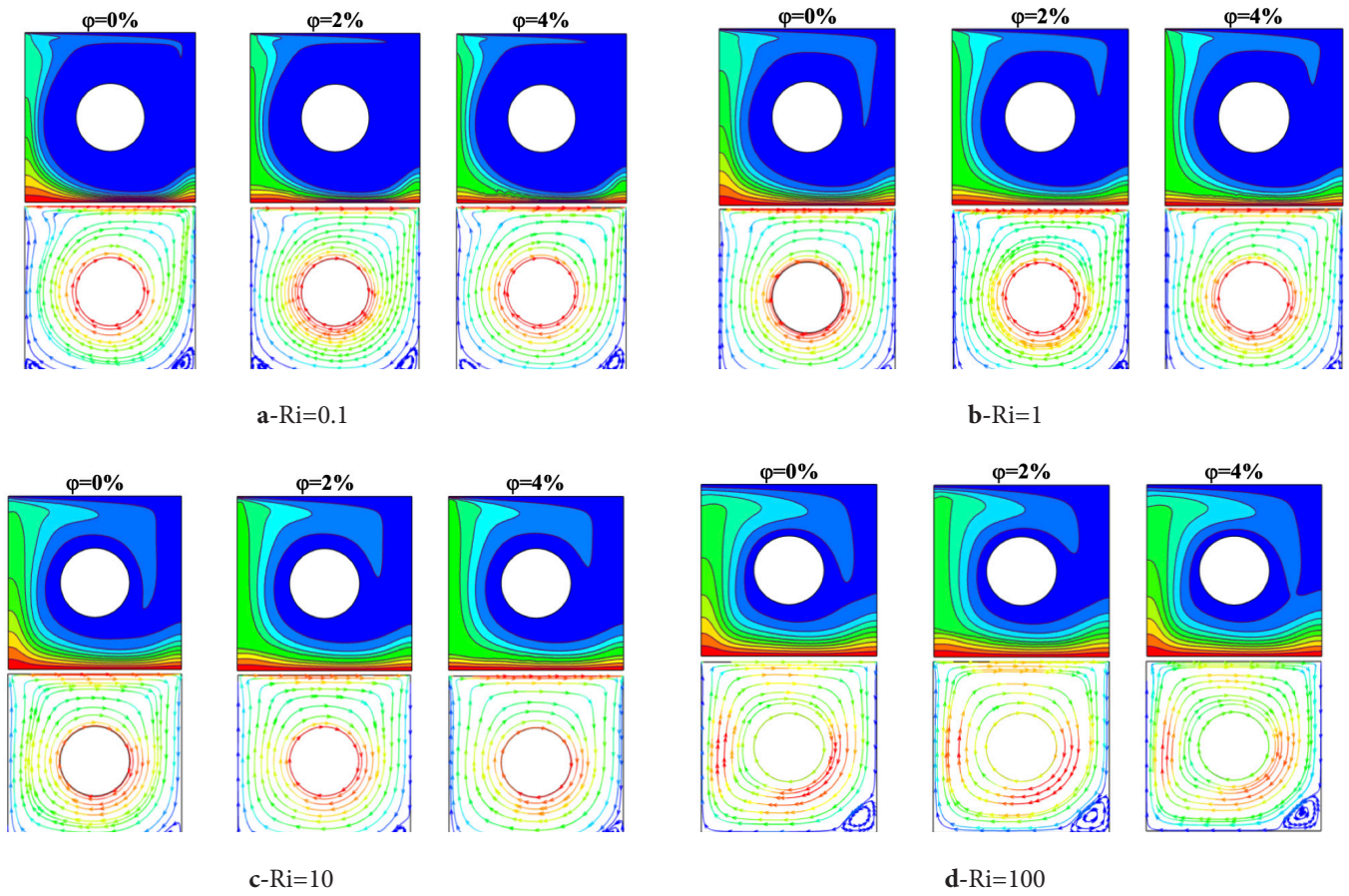

Figure 9. Effect of $Ga@SiO_2$ volume fraction on flow structure and temperature distribution across various Ri ($0.1 \leq Ri \leq 100$)

Figure 10 (a–d) illustrates the local Nu along the hot wall for different Ri and j . Nu drops with increasing Ri for all $Ga@SiO_2$ concentrations, according to the data. Because the velocities of the wall-moving and the cylinder- rotating are reduced, natural convection takes over as the principal heat transfer mechanism, and forced convection is reduced. In addition, the incorporation of $Ga@SiO_2$ enhances heat transfer performance in all the cases considered. Nu distribution along the heated wall presents a parabolic profile, it reaches its peak at about Y=0.65. This variation is primarily related to the imposed asymmetric boundary conditions within the cavity. The results imply that convective heat transfer is notably stronger on the left side of the cavity compared to the right wall. This difference seems to come from stronger buoyancy effects near the left boundary, which are amplified by the thermal and flow conditions in place. On the other hand, the right side has weaker natural convection activity. As the volume ratio of $Ga@SiO_2$ increases, heat transfer is correspondingly enhanced. These results highlight the critical role of boundary conditions in convective heat transfer within confined spaces and demonstrate that $Ga@SiO_2$ significantly improves heat transfer performance.

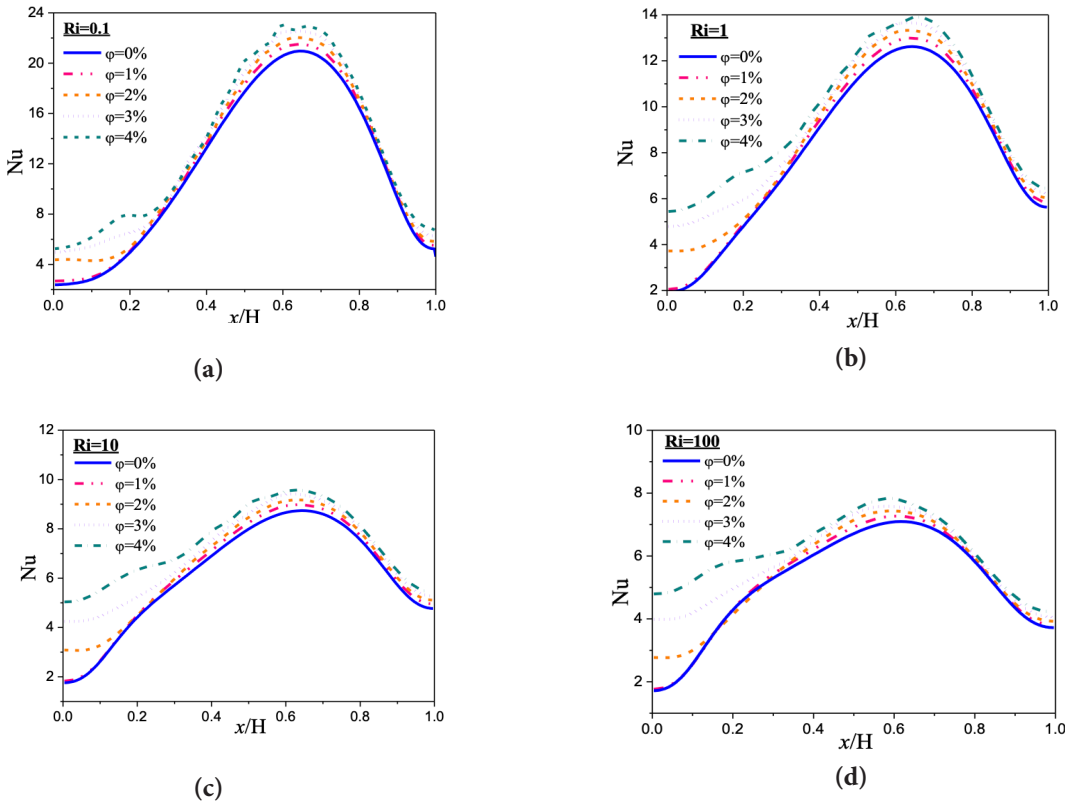

Figure 10. Distribution of Nu along the heated wall for different j and Ri

Figure 11 (a) shows how the heat transfer varies along the heated wall as a function of j for four dissimilar Ri values. It is observed that, for all concentrations of Ga@SiO_2, heat transfer decreases with increasing Ri. At higher Ri values, natural convection becomes the leading heat transfer mechanism, which explains this trend. Adding Ga@SiO_2 improves heat transfer performance across all cases. This improvement in heat transfer is attenuated at higher Ri values due to the dominance of convective effects. Therefore, optimizing thermal performance under different flow conditions depends on selecting an appropriate Ga@SiO_2 concentration. To quantify this enhancement, Figure 11(b) presents the percentage increase in heat transfer owing to the addition of Ga@SiO_2. At φ = 4% and Ri = 10, the most significant improvement is observed, reaching 20.3%. As φ increases, the enhancement becomes more pronounced at lower Ri values (e.g., Ri = 0.1), reaching approximately 15.7% at φ = 4%. For φ values between 1% and 3%, thermal enhancement generally decreases with increasing Ri, except at φ = 4%. Overall, the outcomes indicate that heat transfer performance is governed by both the Ga@SiO_2 concentration and Ri.

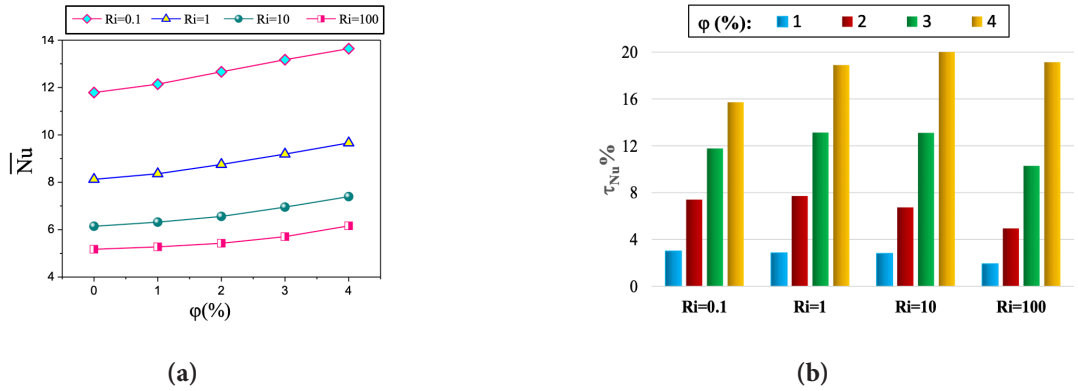

Figure 11. Effect of Ga@SiO_2 concentration on **(a)** and **(b)** Heat transfer enhancement at various Ri

4.2. Comparative Analysis between SiO_2/Water and Ga@SiO_2/Water Nanofluids

This section presents a comparative analysis between SiO_2/water and Ga@SiO_2/water nanofluids under identical operating conditions, with the aim of assessing the effect of nanoparticle type on the thermal performance of the system. The results provide a clear basis for assessing the respective contributions of SiO_2 and Ga@SiO_2 nanoparticles to heat transfer enhancement.

Figure 12 illustrates the Nusselt number distribution along the heated wall at φ = 4% for both nanofluids. It is monitored that the Nusselt number profile of the SiO_2/water nanofluid remains very close to that of the base fluid for all Ri, indicating a limited enhancement effect. In contrast, the Ga@SiO_2/water nanofluid exhibits a noticeable deviation, reaching a maximum difference of up to 175% in comparison to the base fluid. This clearly indicates that the addition of SiO_2 nanoparticles causes to only a marginal advance in heat transfer, whereas the incorporation of Ga@SiO_2 significantly enhances the thermal performance within the cavity.

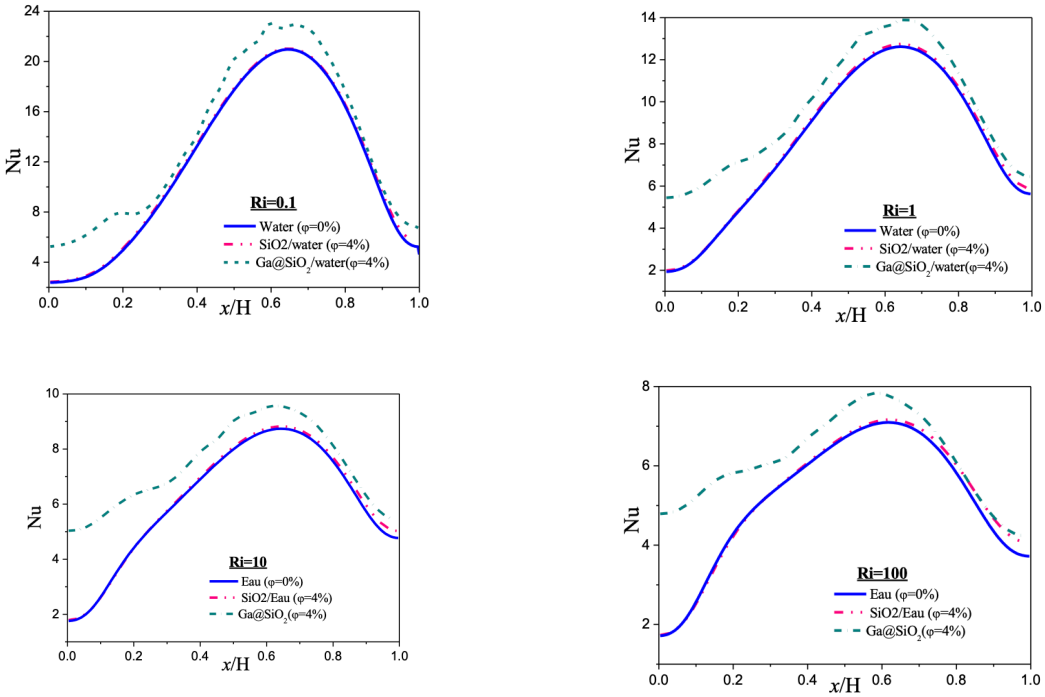

Figure 12. Distribution of Nu Along the Heated Wall for Ga@SiO_2/water and SiO_2/water nanofluids

Further comparison is conducted on variation $\overline{Nu}$ along the heated wall for both fluid types across various φ and Ri, as shown in Figure 13. The consequences obviously demonstrate that the effect of adding SiO_2 nanoparticles is negligible compared to that Ga@SiO_2 for all tested concentrations and Ri.

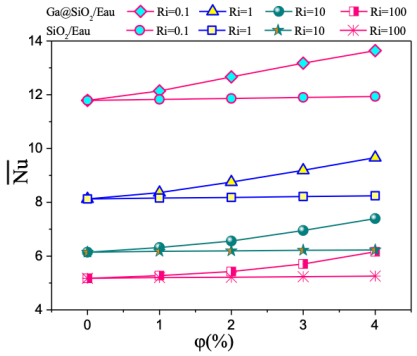

Figure 13. Distribution of $\overline{Nu}$ along the heated wall for the two nanofluid types

To compare the influence of the nanoparticle type on thermal performance, the relative improvement in heat transfer was evaluated and plot in Figure 14. The addition of Ga@SiO_2 nanoparticles indicates to a important enhancement in heat transfer, with a maximum improvement of 20.31% at j=4% and Ri=10. Compared to SiO_2 the improvement is around 1.68%, under the same conditions, which represents 18% performance difference. This discrepancy stems from the contrasting thermophysical properties of the two types of nanoparticles. The adding of SiO_2 nanoparticles improve heat transfer by growing thermal conductivity, where Ga@SiO_2 nanoparticles offer additional advantages due to the latent heat of Ga as a PCM. More effective absorption and redistribution of thermal energy throughout the fluid is made possible by this structure, which allows the storage and release of latent heat within a tight temperature range. The outcome is an enormous improvement in convective heat transfer. In addition, the gallium core is encased in a SiO_2 shell, which increases the nanoparticles' stability and guarantees constant and dependable thermal performance.

It should be noted that the present model relies on steady-state, two-dimensional, and Newtonian assumptions, which may limit the general applicability of the results. Transient effects, three-dimensional flow structures, and possible non-Newtonian behavior are not considered. However, for the range of conditions examined in the current investigation, especially at low particle concentrations (up to 4%), the flow can reasonably be approximated as Newtonian, as commonly reported in the literature. Finally, many countries have made switching to renewable energy sources a top priority due to the need to deal with climate change and reduce carbon emissions [41]. The thermal and technical characteristics of the building materials, the building's operating conditions, the best structural and architectural design solutions, and the climate of the construction site are the main determinants of energy loss in building envelope structures [42]. One of the most important processes in numerous disciplines of engineering is thermal management systems. These applications include electronics cooling, refrigeration, air conditioning, nuclear reactor safety and chemical process intensification. The work is supposed to have significant contribution to these thermal energy fields in the near future.

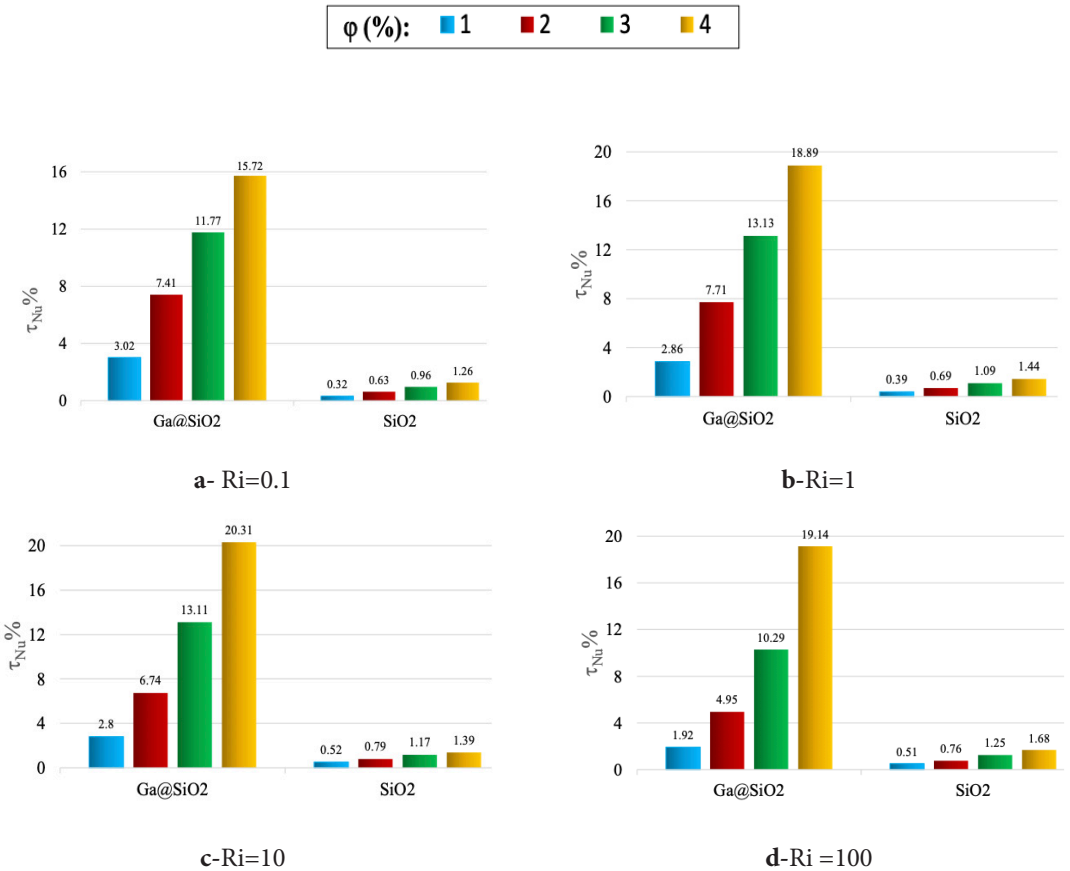

a- Ri=0.1 **b**-Ri=1

c-Ri=10 **d**-Ri =100

Figure 14. Heat transfer enhancement for the two types of nanofluids

5. Conclusion

This study presents a direct comparison between a novel class of NEPCM-based nanofluids and conventional SiO_2 nanoparticles under identical conditions, through numerical research of mixed convection heat transfer in a square cavity. Water-based nanofluids including nano-encapsulated phase change material ($Ga@SiO_2$) are considered over a wide range of Richardson numbers ($0.1 \leq Ri \leq 100$) and nanoparticle volume fractions (0%–4%), and the results are compared with those obtained for conventional SiO_2 nanoparticle suspensions. Key findings are as follows:

a. The thermal and flow field structures of $Ga@SiO_2$ nanofluids are significantly influenced by both Ri and φ. for low Ri values, the performance heat transfer improves as φ increases, while the overall flow structure tends to remain stable because of the dominance of forced convection. Conversely, at higher Ri values, where natural convection becomes more significant, an increase in φ results in noticeable enhancements in both fluid velocity and heat transfer rates.

b. Ri is crucial in determining the relative impacts of forced convection—driven by the moving cylinder and lid—and buoyancy-driven natural convection. Changes in Ri create different vortex patterns and affect the temperature distributions inside the cavity.

c. The distribution of the local Nusselt number shows a noticeable asymmetry along the walls of the cavity, du of the boundary conditions**.**

d. The addition of $Ga@SiO_2$ nanoparticles leads to a heat transfer boost of about 20% when Ri =10 and φ = 4%. This improvement comes from the fact that the thermal conductivity is better, the heat capacity is higher, and there's some latent heat from the phase change material that's wrapped up inside.

e. For pure SiO_2 nanoparticles, the boost is just about 1.7%. This really highlights how $Ga@SiO_2$/water nanofluids are better.

The present study demonstrates that $Ga@SiO_2$/water nanofluids exhibit enhanced heat transfer performance in mixed convection systems. Unlike conventional solid nanoparticles, these materials can store and release thermal energy through latent heat, providing an additional mechanism for thermal regulation. The results indicate the practical engineering relevance of $Ga@SiO_2$/water nanofluids. They enhance heat transfer in lid-driven cavities, making them suitable for electronic cooling applications where efficient thermal management is essential. The observed improvements also suggest potential use in heat recovery systems to increase energy efficiency. Overall, the findings can support the design of compact thermal systems operating under different flow conditions.

Nomenclature

Roman letters

c	Core (subscript)
d	Diameter, m
g	Acceleration of gravity, m/s^2
Ga	Grashof number
k	Thermal conductivity, W/m·K
$1_s/c$	Shell-to-core weight ratio
L_f	Latent heat of fusion J/ kg
Nu	Local Nusselt number
$\overline{Nu}$	Mean Nusselt number
P	Mean static pressure, Pa
Pr	Prandtl number
Re	Reynolds number
Ri	Richardson number
T	Temperature, K
u, v	Velocity components, m/s
U, V	Non-dimensional velocity components
V_m	Velocity magnitude, m/s
V_p	Velocity of the moving walls, m/s
x, y	Dimensional coordinates, m
X, Y	Non-dimensional coordinates

Greek symbols

α	Dimensionless geometric parameter
β	Thermal expansion coefficient, K^{-1}
μ	Viscosity, Pa·s
ρ	Density, kg/m^3
φ	Volume fraction
θ	Dimensionless temperature

Symbols

@	Separator used in core–shell nanoparticle notation

Subscripts

c	Core
f	Base fluid
nf	Nanofluid
p	Particle
s	she
*	Dimensionless quantities

Acknowledgement

The last author, Ahmet Selim Dalkılıç, would like to acknowledge the support from the Scientific Research Department, Azerbaijan University of Architecture and Construction in Azerbaijan, with the permission from the Ministry of Science and Education of the Republic of Azerbaijan under the protocol on international cooperation between YTU and AzUAC dated 16.04.2025.

Declaration of generative ai and ai-assisted technologies in the writing process

During the preparation of this work, the authors used QuillBot to improve the writing and English of some sections. After using this tool/service, the authors reviewed and edited the content as needed, and they take full responsibility for the content of the publication.

Conflict of interests

The authors declare that they have no known competing financial interests or personal relationships that could have appeared to influence the work reported in this paper.

Credit authorship contribution statement

Farida Iachachene: Writing – original draft, Writing – review and editing, Validation, Data curation, Supervision. Cheradi Hanane: Writing – original draft, Writing – review and editing, Formal analysis, Investigation. Leila Saoudi: Writing – review and editing, Formal analysis, Investigation. Ahmet Selim Dalkilic: Writing – review and editing.

References

[1] TOUMZINE, S., & MOULAY ABDELALI, H. (2026). Phase change materials (PCMs) used in buildings: A critical review. Journal of Thermal Engineering, 12(1).

[2] Aljabaır, S., Alesbe, I., & Ibrahım, S. H. (2023). Review on latent thermal energy storage using phase change material. Journal of Thermal Engineering, 9(1), 247-256.

[3] Rai, S. K., Kumar, P., & Panwar, V. (2020). Numerical analysis of influence of geometry and operating parameters on Ledinegg and dynamic instability on supercritical water natural circulation loop. Nuclear Engineering and Design, 369, 110830.

[4] Rai, S. K., Ahlawat, N., Kumar, P., & Panwar, V. (2021). Mathematical modeling and numerical investigation of density wave instability of supercritical natural circulation loop. In E3S Web of Conferences (Vol. 321, p. 04004). EDP Sciences.

[5] Kushwah, A., Kumar, A., & Gaur, M. K. (2025). Techno-economic analysis of solar still with nano-phase change material and heating coil: A novel approach for sustainable development. Journal of Thermal Engineering, 11(2), 476-492.

[6] Rai, S. K., Kumar, P., Panwar, V., Gupta, M. K., Bhatt, D., Kumar, D., ... & Gupta, M. (2025). A comprehensive investigation of computational analysis on flow characteristics, stability and safe limits of a supercritical natural circulation loop for different heating power profiles. Nuclear Engineering and Technology, 103858.

[7] R, R.K., N, C.K.N., ALI, A.B., L, B., AL-NUSSAIRI, A.K.J., B P, V., KHAN, A., SMERAT, A., KHAN, A. (2026). Enhancement of exhaust manifolds using hybrid Graphene-TiO_2 nano fluids in multi-cylinder diesel engines: A CFD study on TiO_2 advantages. Journal of Thermal Engineering, 12(2), 702-722. https://doi.org/10.14744/thermal.0001111

[8] AMIRI, M., KARIMI, R., & ABBASPOUR, I. (2026). Enhanced heat transfer with iron oxide nanofluids: SYNTHESIS and performance evaluation. Journal of Thermal Engineering, 12(1).

[9] PRIYADARSHANA, V. V., INDURANGA, A., GALPAYA, C., SAMARATHUNGA, A. I., & KOSWATTAGE, K. (2025). A review on enhancement of solar photovoltaic (PV) system performance with water-based nano-fluid cooling systems. Journal of Thermal Engineering, 11(4).

[10] Mozafary, B., Akbar, A., Aranı, A., Nooshabadı, G. A. S., & Salımı, M. (2024). Brownian motion models effect on the nanofluid fluid flow and heat transfer in the natural, mixed, and forced convection. Journal of Thermal Engineering, 10(1), 88-100.

[11] Husseın, A. M., Awad, A. T., & Alı, H. H. M. (2024). Evaluation of the thermal efficiency of nanofluid flows in flat plate solar collector. Journal of Thermal Engineering, 10(2), 299-307.

[12] Ramadhan, A. I., Saptaji, K., Hendrawati, T. Y., Sari, A. M., Umar, E., Aziz, A., ... & Firmansyah, F. (2025). Heat transfer performance analysis of green nanofluids as coolant in automotive radiator for motorcycle engine. J Adv Res Fluid Mech Therm Sci, 126, 214-225.

[13] Gao, Y., Liu, H., Gui, H., Yao, C., Zhang, G., & Liang, F. (2024). Solid-liquid phase change materials microcapsules: Synthesis strategies, thermal storage and beyond. Progress in Natural Science: Materials International.

[14] Mendes, P. C., Song, Y., Ma, W., Gani, T. Z., Lim, K. H., Kawi, S., & Kozlov, S. M. (2023). Opportunities in the design of metal@ oxide core-shell nanoparticles. Advances in Physics: X, 8(1), 2175623

[15] Haddad, Z. (2025). A comprehensive review of micro/nano-encapsulated phase change material-based fluids: Modeling, properties, and heat transfer enhancement. Renewable and Sustainable Energy Reviews, 216, 115640.

[16] [16]Albdour, S. A., Haddad, Z., Sharaf, O. Z., Alazzam, A., & Abu-Nada, E. (2022). Micro/nano-encapsulated phase-change materials (ePCMs) for solar photothermal absorption and storage: Fundamentals, recent advances, and future directions. Progress in Energy and Combustion Science, 93, 101037.

[17] Zhou, Y., Yang, Z., Zou, S., Wang, L., Yang, C., & Chen, R. (2025). Study on the comprehensive effects of microencapsulated phase change materials on the thermodynamic properties and long-term durability of concrete. Construction and Building Materials, 500, 144170.

[18] Ren, C., Gui, X., Wang, Y., Xiang, L., Tang, B., Shi, S., ... & Wu, X. (2025). Preparation of Ag@ CFC/EP composites with excellent thermal management performance via electroless silver plating on polydopamine-modified carbon fiber/carbon felt. Composites Communications, 102552.

[19] Wang, Z., Miao, T., Zhang, Y., Chang, C., Wang, R., Lang, K., & Wang, F. (2026). Enhancement on thermal properties of graphene/paraffin phase change microcapsules with connected thermal network. International Journal of Heat and Mass Transfer, 255, 127780.

[20] Iachachene, F., Achab, L., & Cheradi, H. (2025). ENHANCING HEAT TRANSFER WITH NEW HYBRID NANOFLUIDS TYPE CORE@ SHELL NANOPARTICLES. Journal of Enhanced Heat Transfer, 32(2).

[21] Gao, L., Cui, Y., Li, J., Wu, Z., & Li, H. (2026). Thermal conductivity enhanced n-hexadecane@ PUA/Cu phase change microcapsules for temperature-regulating energy storage mortar. Journal of Energy Storage, 150, 120417.

[22] Xu, Z., & Sheng, D. (2026). 1-Octadecanol/magnesium hydroxide phase change microcapsules with heat storage and thermal regulation properties. Journal of Energy Storage, 141, 119214.

[23] Alasfoor, O. F., Sherif, S. A., & Kalendar, A. (2026). Sensitivity Analysis of Microencapsulated Phase Change Material Slurry With Arbitrary Particle Shapes. Journal of Solar Energy Engineering, 148(2), 021006.

[24] Ho, C. J., Chang, P. C., Yan, W. M., & Amani, M. (2018). Microencapsulated n-eicosane PCM suspensions: Thermophysical properties measurement and modeling. International Journal of Heat and Mass Transfer, 125, 792-800.

[25] Dutkowski, K., & Kruzel, M. (2025). Experimental Studies on the Critical Reynolds Number in the Flow of a Microencapsulated Phase Change Material Slurry. Energies, 18(6), 1520.

[26] Yu, L., Jiang, Y., Yang, B., Lv, X., Liu, H., Liu, G., & Wang, X. (2025). Reverse emulsion-templated nanoencapsulation of NaNO3 with crystalline TiO2 shell for high-temperature heat energy storage and thermal corrosion resistance. Journal of Energy Storage, 128, 117277.

[27] Ghalambaz, M., Chamkha, A. J., & Wen, D. (2019). Natural convective flow and heat transfer of nano-encapsulated phase change materials (NEPCMs) in a cavity. International journal of heat and mass transfer, 138, 738-749.

[28] Ghalambaz, M., Groşan, T., & Pop, I. (2019). Mixed convection boundary layer flow and heat transfer over a vertical plate embedded in a porous medium filled with a suspension of nano-encapsulated phase change materials. Journal of Molecular Liquids, 293, 111432.

[29] Ahmed, S. E., & Raizah, Z. A. (2021). Analysis of the entropy due to radiative flow of nano–encapsulated phase change materials within inclined porous prismatic enclosures: Finite element simulation. Journal of Energy Storage, 40, 102719.

[30] Raizah, Z., & Aly, A. M. (2021). Double-diffusive convection of a rotating circular cylinder in a porous cavity suspended by nano-encapsulated phase change materials. Case Studies in Thermal Engineering, 24, 100864.

[31] Sadr, A. N., Shekaramiz, M., Zarinfar, M., Esmaily, A., Khoshtarash, H., & Toghraie, D. (2022). Simulation of mixed-convection of water and nano-encapsulated phase change material inside a square cavity with a rotating hot cylinder. Journal of Energy Storage, 47, 103606

[32] Qasem, N. A., Abderrahmane, A., Khetib, Y., Rawa, M., Abdulkadhim, A., Eldin, S. M., & Younis, O. (2023). Mixed convection within trapezoidal-wavy enclosure filled with nano-encapsulated phase change material: effect of magnetohydrodynamics and wall waviness. Case Studies in Thermal Engineering, 42, 102726.

[33] Herouz, K., Laidoudi, H., Aissa, A., Mourad, A., Guedri, K., Oreijah, M., & Younis, O. (2023). Analysis of nano-encapsulated phase change material confined in a double lid-driven hexagonal porous chamber with an obstacle under magnetic field. Journal of Energy Storage, 61, 106736.

[34] Iachachene, F., Halouane, Y., & Achab, L. (2023). Heat transfer enhancement in lid-driven cavity with rotating cylinder: exploring NEPCMs and magnetic field effects. International Communications in Heat and Mass Transfer, 149, 107095.

[35] Dahani, Y., Hasnaoui, S., Chtaibi, K., El Mansouri, A., Filahi, I., Amahmid, A., & Hasnaoui, M. (2025). Optimization of heat transfer in water-nepcm filled cavities through cylinder rotation and size variation. Computational Thermal Sciences: An International Journal, 17(6).

[36] Chiu, S. H., Baharfar, M., Chi, Y., Widjajana, M. S., Cao, Z., Allioux, F. M., ... & Kalantar-Zadeh, K. (2023). Exploring electrical conductivity of thiolated micro-and nanoparticles of gallium. Advanced Intelligent Systems, 5(5), 2200364.

[37] Alisetti, E. L., & Roy, S. K. (2000). Forced convection heat transfer to phase change material slurries in circular ducts. Journal of thermophysics and heat transfer, 14(1), 115-118.

[38] Uniyal, A., Bose, S., Kumar, D., Prajapati, Y. K., Ranakoti, L., & Rai, S. K. (2025). Evaluation of thermal efficiency in coaxial evacuated tube collectors: Influence of shadowing and phase change material selection. Journal of Energy Storage, 120, 116492.

[39] Khanafer, K., & Aithal, S. M. (2017). Mixed convection heat transfer in a lid-driven cavity with a rotating circular cylinder. International Communications in Heat and Mass Transfer, 86, 131-142.

[40] Xu, B., Li, B. Q., & Stock, D. E. (2006). An experimental study of thermally induced convection of molten gallium in magnetic fields. International journal of heat and mass transfer, 49(13-14), 2009-2019.

[41] Samira, A., & Reyhan, A. (2025). Renewable energy transition strategy. Elmi Əsərlər/Scientific Works of Azerbaijan University of Architecture and Construction, (1).

[42] Samira, A. (2022). Normalized thermal-technical parameters of external constructions affecting the energy efficiency of the building. Elmi Əsərlər/Scientific Works of Azerbaijan University of Architecture and Construction, (2).